Energy transfer in nanochannels

G. Calzaferri

Department of Chemistry and Biochemistry, University of Bern
Freiestrasse 3, CH-3012 Bern, Switzerland

Summary. — Artificial photonic antenna systems have been built by incorporating organic dyes into one-dimensional nanochannel materials. We have been focusing on zeolite L as a host in most of our experiments since it has proved to be very versatile. Zeolite L consists of strictly parallel channels arranged in a hexagonal framework. The size and aspect ratio of the colorless crystallites can be tuned over a wide range. Its one-dimensional channels can be filled with suitable organic guests. Geometrical constrains of the host structure lead to supramolecular organization of the guests in the channels. Thus very high concentration of non- or very weakly interacting dye molecules can be realized. A special twist is added to these systems by plugging the channel openings with a second type of fluorescent dye, which we call stopcock molecule. The two types of molecules are precisely tuned to each other; the stopcocks are, *e.g.*, able to accept excitation energy from the dyes inside the channel, but cannot pass it back. The supramolecular organization of dyes inside the zeolite channels is what we call the first stage of organization. It allows light harvesting within the volume of a dye-loaded zeolite L crystal and also radiationless energy transport to either the cylinder ends or to the centre. One-dimensional excitation energy transport was observed in these dye-zeolite L guest-host materials. The second stage of organization represents the coupling to an external acceptor or donor stopcock fluorophore at the ends of the zeolite L channels, which can then trap or inject electronic excitation energy. The third stage of organization is obtained by interfacing the material to an external device via a stopcock intermediate. We explain the theoretical and conceptual background of these systems by using a simple approach which promotes the intuitive understanding. The focus is on molecules, materials and phenomena in which the interaction energy between the donor and the acceptor is small in the electronic ground state and also in the electronically excited state. The chromophores consist essentially of a positively charged backbone and some delocalized electrons. The energy of an absorbed photon is transformed into kinetic energy of one of these electrons. This fast moving electron causes an oscillating electromagnetic field. A neighboring molecule bearing states that are in resonance can interact. We consider systems in which the "optical electrons"

associated with the individual component molecules (or chromophoric units) preserve essentially their individual character and we describe the consequences of the interaction under this condition. The outcome of the resulting electronic transitions dipole moment coupling is Förster resonance energy transfer (FRET) and exciton splitting.

PACS `71.35.-y` – Excitons and related phenomena.
PACS `81.07.Pr` – Organic-inorganic hybrid nanostructures.
PACS `82.75.-z` – Molecular sieves, zeolites, clathrates, and other complex solids.
PACS `82.75.Mj` – Measurements and simulation of properties (optical, structural) of molecules in zeolites.

1. – Introduction

Atoms, molecules, clusters, and solids can exist in many different states in which they have the possibility to exchange energy. Exchange of any kind of energy between atoms and molecules is responsible for the very short lifetime of excited rotational and vibrational states of molecules in gases at medium and at high pressure and especially in condensed phase [1]. There are cases where near-field interactions are governing the energy exchange processes, while usually mechanical contact or some overlap of the electronic wave functions between the interacting molecules is needed. Near-field interaction occurs at distances shorter than half the wavelength of a free photon. In molecular crystals and in some polymers which contain the right type and arrangement of chromophores, energy quanta can be transported as bound electron-hole packages over considerable distances. Exchange of energy between molecules at larger distances can either occur via electronic excitation energy migration among equal molecules or via emission and absorption of photons. The latter process is considered as trivial mechanism [2-5].

Green plants have developed very sophisticated tools for trapping and transporting electronic excitation energy in their antenna system. Photosynthesis is the process by which plants, some bacteria, and some protistans use the energy from sunlight to produce sugar which cellular respiration converts into ATP, the "fuel" used by all living things. The conversion of sunlight energy into chemical energy is associated with the actions of the green pigment chlorophyll. Most of the chemistry associated with photosynthesis is understood at a reasonably precise level and although refinements continue to be made, the basic understanding is in place [6].

The detailed structure of the antenna system of purple bacteria has been resolved. It consists of regular arrangements of chlorophyll molecules held at fixed positions by means of proteins [7]. Light absorbed by any of these chlorophyll molecules is transported to the reaction center, providing the energy necessary for the chemical processes to be initiated. A green leaf consists of millions of such well-organized antenna devices. Recreating this system in the laboratory would be a hopeless task—at least regarding the current possibilities of chemists. What can be done? First we should understand the basic principles that govern transport of electronic excitation energy. Fortunately, this understanding is very advanced. It goes back to the pioneering work of Theodor Förster [4]. A chlorophyll molecule consists essentially of a positively charged backbone and some delocalized electrons. The energy of an absorbed photon is transformed into kinetic energy of one of these delocalized electrons. This fast moving electron causes

an oscillating electromagnetic field. A neighboring acceptor molecule A, bearing states that are in resonance with the excited state of the donor D^*, can take over the excitation energy. Radiationless electronic excitation energy transfer is due to very weak interaction between excited configurations of the initial state $(D^* \ldots A_i)$ and that of the final state $(D \ldots A_i{}^*)$.

$$(1) \qquad\qquad (D^* \ldots A_i) \xrightarrow{k_{\mathrm{EnT}}(i)} (D \ldots A_i{}^*).$$
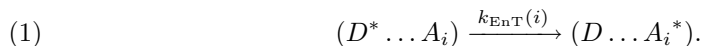
In such a system the "optical electrons" associated with individual component molecules (or chromophoric units) preserve essentially their individual characteristic. The donor D and the acceptor A can be the same sort of molecules or they can be different. Förster observed that the rate constant k_{EnT} for the transfer from one electronic configuration to the other can be expressed as a product of three terms: a geometrical term G that describes the distance and angular dependence of the rate constant, a term DA specific for the chromophores involved, taking into account the resonance condition and the electronic transition dipole moments (ETDM) of the donor and the acceptor, and a factor S which takes the environment into account:

$$(2) \qquad\qquad k_{\mathrm{EnT}} \propto G \cdot DA \cdot S.$$

Our design of a model that mimics the key functionality of the antenna system of green plants was inspired by experience we had with different zeolite materials [8,9]. Properties of molecules, complexes and clusters inside the cavities and channels—apart from the interest in catalysis—have been investigated by several authors [10]. We reasoned that a one-dimensional channel system has the advantage of being the simplest possible choice. This is illustrated in fig. 1. The donor molecules are represented in green and the acceptors in red (colour on-line version). The donor that has been excited by absorbing an incident photon transfers its electronic excitation to an unexcited neighbor. After series of such steps, the electronic excitation reaches a luminescence trap (acceptor molecule) and is then released as fluorescence. The acceptors are thought to mimic the "entrance of the reaction center" of the natural antenna. The dimensions given in fig. 1 correspond to the pore opening and the distance between the centers of two channels in zeolite L. According to Förster theory, the largest energy transfer rate constant is observed if the ETDM are oriented parallel to the channel axis. Electronic excitation energy transport can be extremely fast in such systems because of its low dimensionality.

Different materials bearing one-dimensional channels can be envisaged for realizing the situation explained in fig. 1. We found that zeolite L is a good host for supramolecular organization of dyes because synthesis of zeolite L crystals of different morphology in the size range of 30 nm up to about 10000 nm is well established, which means that it is possible to cover about 7 orders of magnitude in terms of volume [11]. We therefore focus on systems based on zeolite L as a host. The theoretical reasoning is, however, also valid for other host materials with similar properties. The structure and morphology of zeolite L is explained in fig. 2. The primary building units are TO_4 tetrahedra where T is equal to Al or Si. Connecting them by means of oxygen bridges one obtains the hexagonal arrangement of the channels. The composition of zeolite L is $(M^+)_9[(AlO_2)_9(SiO_2)_{27}] \times nH_2O$, where M^+ are monovalent cations, compensating the negative charge resulting from the aluminium atoms. n is 21 in fully hydrated materials, and 16 at about 22% relative humidity [12].
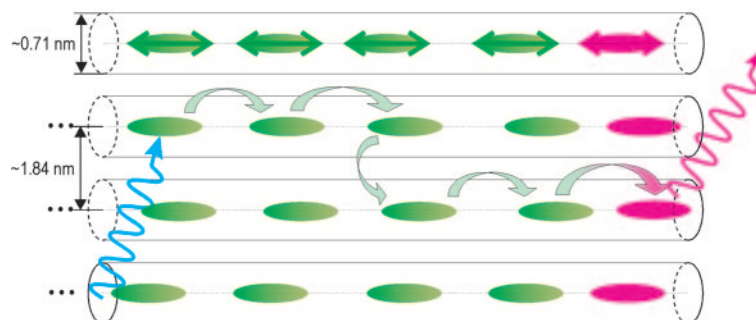
Fig. 1. – (Colour on-line) Schematic view of an artificial photonic antenna. The chromophores are embedded in the channels of the host. The green dyes act as donor molecules which absorb the incoming light and transport the excitation via Förster energy transfer to the red acceptors shown at the ends of the channels on the right. The process can be analyzed by measuring the emission of the red acceptors and comparing it with that of the donors.

It is useful to imagine zeolite L as consisting of a bunch of strictly parallel channels as shown in fig. 2D [13]. The channels have a smallest free diameter of about 7.1 Å, the largest diameter inside is 12.6 Å. The distance between the centers of two channels is 18.4 Å. Each zeolite L crystal consists of a large number n_{ch} of channels which can be estimated as follows:

$$(3) \qquad n_{ch} = 0.267(d_Z)^2,$$

where d_Z is the diameter of the crystal in nm. For example, a crystal of 600 nm diameter consists of nearly 100000 strictly parallel channels. The ratio of the void space available in the channels with respect to the total volume of a crystal is about 0.26. An important consequence is that zeolite L allows realizing extremely high concentrations of well-oriented molecules that behave essentially as monomers. A 30 nm crystal can
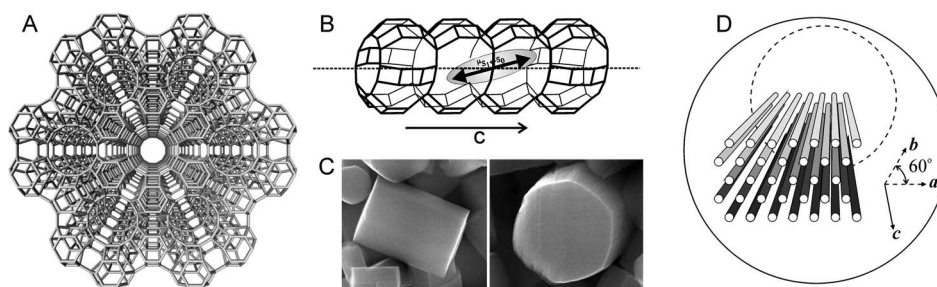

Fig. 2. – Zeolite L. A) Top view of the framework of zeolite L, illustrating the hexagonal structure. It shows a channel surrounded by six neighboring channels. B) Side view of a channel that consists of 0.75 nm long unit cells with a van der Waals opening of 0.71 nm at the smallest and 1.26 nm at the widest place. The double arrow indicates the ETDM of the molecule. C) SEM image of zeolite L crystals with a diameter of about 600 nm. D) Schematic view of the channels. The center-to-center distance between two channels is 1.84 nm.
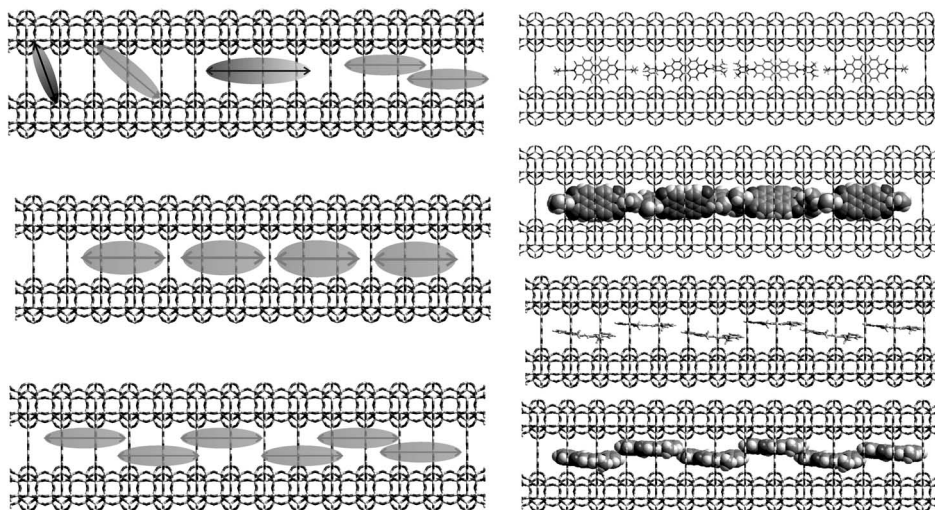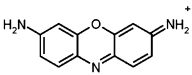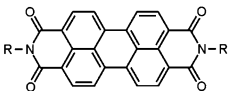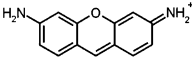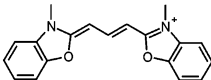
Fig. 3. – Packing of dyes in the channel. Left: simplified view of different orientations and two arrangements of molecules in a channel. The orientation of the ETDM is indicated by a double arrow. Top: the molecule on the left is small enough to fit into one unit cell and its shape is such that the ETDM is oriented nearly perpendicular to the channel axis. Then we see a molecule that occupies two unit cells and is oriented at about 45°. The next molecule is so large that it can only align parallel to the c-axis of the crystal. On the right we illustrate a situation where two molecules come so close that their orientation and their optical properties are influenced by the packing. Middle: orientation of large molecules which align parallel to the channel axis because of their size and their shape. Bottom: stacking of molecules of appropriate size and shape, leading to excitonic states. Right: dense packing of the perylene dye PR149 (upper) and of cyanine dye PC21 (lower).

bear nearly 5000 dye molecules that occupy 2 u.c., while a 60 nm crystal can host nearly 40000. This is extremely interesting!

Here we focus on situations where molecules behave in the states of interest as individuals, which means that the "optical electrons" associated with the chromophoric units preserve essentially their individual characteristic, who, however, can communicate with each other. We are interested in molecules that are so large that they cannot pass each other inside of the channels and that cannot sit on top of each other, as illustrated in fig. 3 where we show a simplified view of different orientations and two arrangements of molecules in a channel. The geometrical constraints imposed by the host which determine the orientation of the dye molecules inside the channels and hence the orientation of the ETDM, indicated by a double arrow, is schematically explained in fig. 3 (left). Exciton splitting becomes important at sufficiently short distance between the ETDM of neighboring molecules.

Försters theory leads to a simple expression for the energy transfer rate constant that contains only experimentally accessible parameters. This is of great value. The theory has been generalized in order to also meet more complex situations [2, 3]. Here we explain the rate equation for FRET by following the arguments given in the original work of Förster and we describe exciton coupling based on Davydov's theory [4, 14, 15]. The results have been found to be very useful for designing and understanding organize systems based on nanochannel materials [9, 13, 16, 17]. The discussion is restricted to
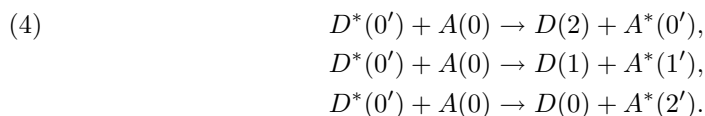
TABLE I. – *Formula and abbreviations of dyes.*

abbreviation	structural formula	abbreviation	structural formula
Ox		Peryl	
Py		PR 149	
Pc21			

one-photon processes and ambient temperature conditions. This means that processes in which two or more electronically excited molecules interact with each other leading to phenomena such as annihilation processes, super radiance, lasing and others but also very low temperature situations where shallow traps may be important are not discussed. Energy transfer is abbreviated as EnT in order to distinguish from electron transfer, for which ET has often been used. Table I shows the structure and the abbreviations of the dyes discussed in this paper.

2. – Electronic transion moment coupling

For excitation energy transfer from an electronically excited molecule D^* to an acceptor A, some interaction between the two molecules is required. Energy transfer can take place if the acceptor molecule possesses transitions which are isoenergetic with those of the excited donor. Transitions between states which are in resonance are abbreviated as RET for resonance energy transfer.

We assume as an illustrative example, fig. 4, that the energy separation between two vibrational states $(v, v + 1)$ of the donor and $(v', v' + 1)$ of the acceptor is the same. We further assume that the energy difference ΔE between the electronic $(0,0')$ transitions of D and A is twice this separation. ΔE reflects only fluctuations in the environment and temperature if the donor and the acceptor are the same type of molecules. The following RET processes can take place:

$$
\begin{aligned}
D^*(0') + A(0) &\rightarrow D(2) + A^*(0'), \\
D^*(0') + A(0) &\rightarrow D(1) + A^*(1'), \\
D^*(0') + A(0) &\rightarrow D(0) + A^*(2').
\end{aligned}
\tag{4}
$$

Transfer of electronic excitation energy can result from different interaction mechanisms. Considering that only two electrons are involved in a transition, one on D and one on A, the antisymmetric electronic wave functions of the initial excited state Ψ_i (D excited but not A) and of the final excited state Ψ_f (A excited but not D) can be expressed as
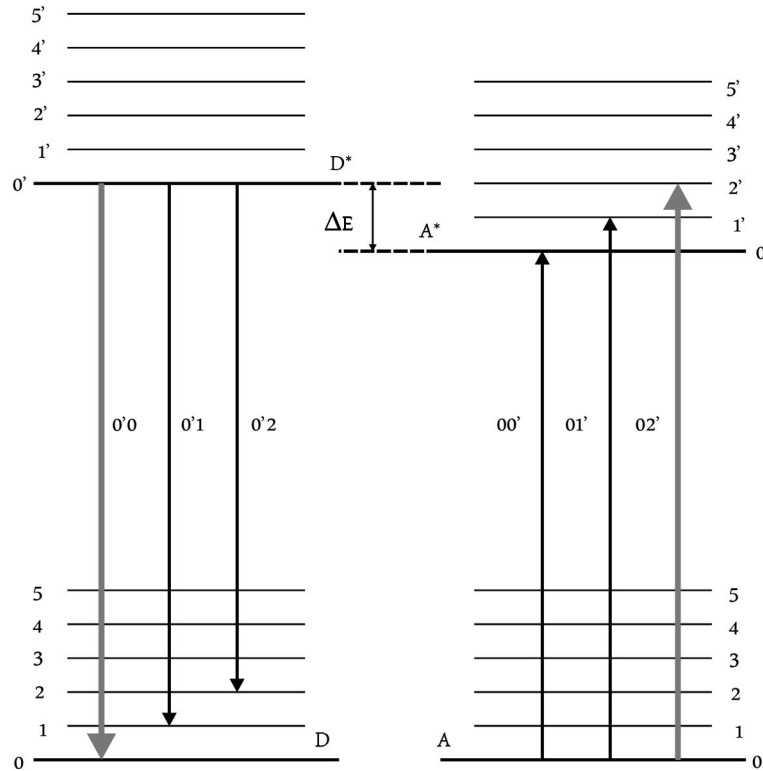
Fig. 4. – Energy levels of a donor molecule D and an acceptor molecule A. The vibrational states in the electronic ground state are labeled as 0, 1, 2, etc. and those in the excited state as $0'$, $1'$, $2'$, etc. The arrows indicate electronic transitions for which the pairs $(0'2; 00')$, $(0'1; 01')$ and $(0'0; 02')$ are in resonance.

follows, where the numbers 1 and 2 refer to the involved electrons:

$$\text{(5)} \qquad \Psi_i = \frac{1}{\sqrt{2}}(\Psi_{D^*}(1)\Psi_A(2) - \Psi_{D^*}(2)\Psi_A(1)),$$

$$\text{(6)} \qquad \Psi_f = \frac{1}{\sqrt{2}}(\Psi_D(1)\Psi_{A^*}(2) - \Psi_D(2)\Psi_{A^*}(1)).$$

The interaction term β between the initial and the final state is

$$\text{(7)} \qquad \beta = \langle \Psi_i | H' | \Psi_f \rangle.$$

H' is the perturbation part of the Hamiltonian

$$\text{(8)} \qquad \hat{H} = \hat{H}_{D^*} + \hat{H}_A + H'.$$

Inserting (5) and (6) in (7) we obtain

$$\text{(9)} \quad \beta = \left\langle \frac{1}{\sqrt{2}}(\Psi_{D^*}(1)\Psi_A(2) - \Psi_{D^*}(2)\Psi_A(1)) \middle| H' \middle| \frac{1}{\sqrt{2}}(\Psi_D(1)\Psi_{A^*}(2) - \Psi_D(2)\Psi_{A^*}(1)) \right\rangle.$$

This expression can be divided in two parts:

(10) $\quad \langle \Psi_{D^*}(1)\Psi_A(2)|H'|\Psi_D(1)\Psi_{A^*}(2)\rangle = \langle \Psi_{D^*}(2)\Psi_A(1)|H'|\Psi_D(2)\Psi_{A^*}(1)\rangle = \beta_{\mathrm{C}},$

(11) $\quad \langle \Psi_{D^*}(1)\Psi_A(2)|H'|\Psi_D(2)\Psi_{A^*}(1)\rangle = \langle \Psi_{D^*}(2)\Psi_A(1)|H'|\Psi_D(1)\Psi_{A^*}(2)\rangle = \beta_{\mathrm{ex}}.$

Hence, β can be written as a sum of two terms:

$$(12) \qquad \qquad \beta = \beta_{\mathrm{C}} - \beta_{\mathrm{ex}}.$$

The Coulomb term β_{C} describes a situation in which the initially excited electron on D^* returns to the ground-state orbital, while an electron on A is simultaneously promoted to the excited state. The exchange term β_{ex} describes a situation which can be understood as an exchange of two electrons, one on D and one on A. The Coulomb and the exchange interaction lead to two distinctly different EnT mechanisms, illustrated in fig. 5. We observe that an exchange of electrons between D and A change takes place in the exchange interaction. This is not the case in the Coulomb mechanism where no electrons are exchanged. The exchange term β_{ex} represents the electrostatic interaction between the charged clouds. In order not to vanish, overlap of the electron clouds is a prerequisite and, hence, energy transfer due to exchange interaction requires overlap of the wave functions of D^* and A, similar as in electron transfer reactions. This is a short-range interaction. For two electrons separated by a distance r_{12} in $D^* \ldots A$, the perturbation H'_{ex} is

$$(13) \qquad \qquad H'_{\mathrm{ex}} = \frac{e^2}{4\pi\varepsilon_0} \frac{1}{r_{12}},$$

where e is the elementary charge of an electron and ε_0 the vacuum permittivity [5].

The Coulomb term can be expanded into a sum of terms (multipole-multipole series)

$$(14) \qquad \qquad \beta_{\mathrm{C}} = V_{dd} + V_{qd} + V_{dq} + V_{qq} + \ldots,$$

where V_{dd} is the dipole-dipole interaction, V_{qd} the quadrupole-dipole interaction and so on. We focus on situations where the dipole-dipole interaction term between the ETDM μ_{D^*D} and μ_{AA^*} of D and A for the transitions $D^* \to D$ and $A \to A^*$ in an environment of refractive index n is dominant. The perturbation H'_{C} can then be expressed by means of eq. (15), where l_{D^*} and l_A are the positions of the ETDM which are at distance R_{D^*A} and where κ_{D^*A} takes the relative orientation of the ETDM of the donor and the acceptor into account, see the scheme in fig. 6.

$$(15) \qquad \qquad H'_{\mathrm{C}} = \frac{e^2}{4\pi\varepsilon_0 n^2} \frac{1}{R_{D^*A}{}^3} l_{D^*} l_A \kappa_{D^*A},$$

$$(16) \qquad \qquad \kappa_{D^*A} = \sin\theta_1 \sin\theta_2 \cos\phi_{12} - 2\cos\theta_1 \cos\theta_2.$$

The rate constant k_{EnT} for electronic excitation energy transfer in the weak-coupling limit can be expressed according to Fermi's Golden rule as follows [2]:

$$(17) \qquad \qquad k_{\mathrm{EnT}} = \frac{2\pi}{\hbar} \beta_{\mathrm{C}}{}^2 \rho.$$
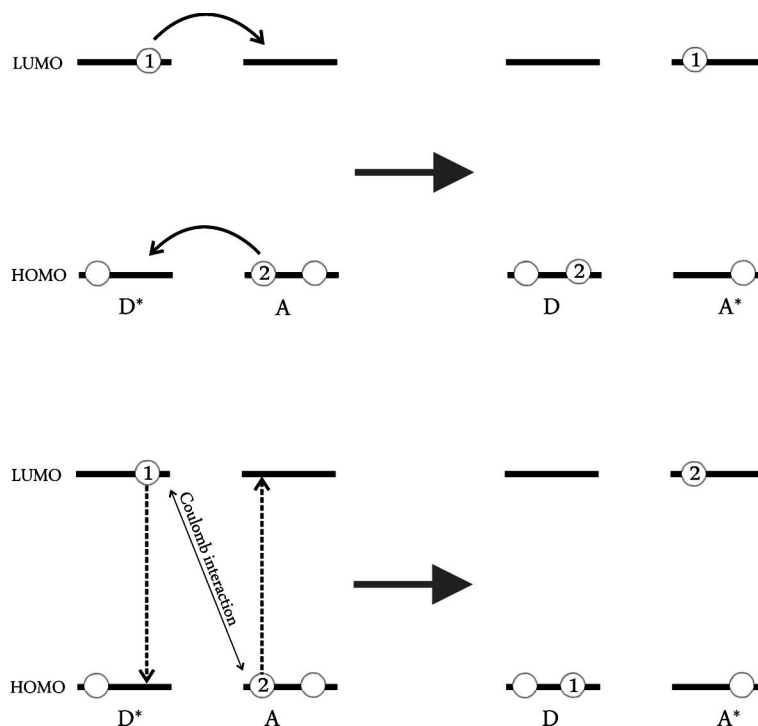
Fig. 5. – Electronic excitation energy transfer. Representation of the exchange (upper) and the Coulomb interaction mechanism (lower). HOMO and LUMO refer to the highest occupied molecular orbital and to the lowest unoccupied molecular orbital, respectively.

Fig. 6. – Angles describing the relative orientation of the ETDM of two molecules, μ_1 and μ_2. The numbers 1 and 2 refer not only to the corresponding electrons but are also used to identify the two species. Top: representation of the ETDM as oscillators. Bottom: vector representation of the ETDM.

ρ is a measure of the density of the interacting initial $D^* \ldots A$ and final $D \ldots A^*$ states. It is related to the overlap between the emission spectrum of the donor and the abs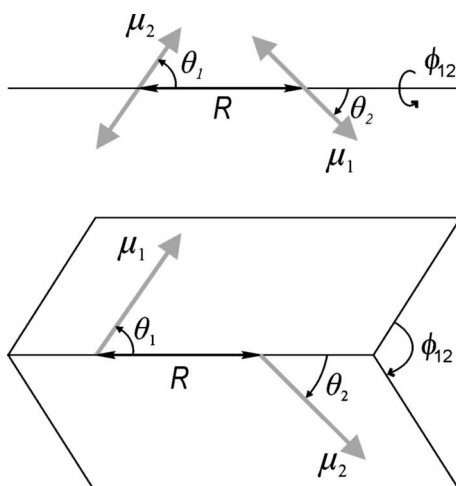orption spectrum of the acceptor. Direct evaluation of eq. (17) by means of numerical quantum chemical calculations of different degrees of sophistication has been performed [18, 19] and intermolecular electronic excitation energy transfer in a confined space has been examined [20].

2`1. *Weak interaction between a molecule in an electronically excited state and a molecule in the ground state*. – For very weak interaction between excited and unexcited molecules, *e.g.*, less than $100\,\mathrm{cm}^{-1}$, the electronic spectrum of a mixture of donors and acceptors, measured under ambient conditions, will be almost an exact superposition of the separate spectra of diluted solutions of donors and of acceptors. Stronger interactions lead to exciton splitting. In order to evaluate the rate constant k_{EnT} for excitation energy transfer from an electronically excited donor D^* and an acceptor A, we must calculate the product $\beta_C{}^2 \rho$, according to eq. (17). The wave functions for the initial (i) and the final (f) states and the perturbation Hamiltonian H'_{C} are given in eqs. (18), (19) and (15).

$$\text{(18)} \qquad \Psi_i = \Psi_{D^*} \Psi_A,$$

$$\text{(19)} \qquad \Psi_f = \Psi_D \Psi_{A^*}.$$

Inserting this in

$$\text{(20)} \qquad \beta_{\mathrm{C}} = \langle \Psi_i | H'_{\mathrm{C}} | \Psi_f \rangle,$$

we can write

$$\text{(21)} \qquad \beta_{\mathrm{C}} = \frac{1}{4\pi\varepsilon_0 n^2} \frac{1}{R_{DA}{}^3} |\langle \Psi_{D^*} | el_D | \Psi_D \rangle| |\langle \Psi_A | el_A | \Psi_{A^*} \rangle| \kappa_{D^* A}.$$

The two matrix elements are equal to the ETDM $\mu_{D^* D}$ and μ_{AA^*}:

$$\text{(22)} \qquad \mu_{D^* D} = \langle \Psi_{D^*} | el_D | \Psi_D \rangle,$$

$$\text{(23)} \qquad \mu_{AA^*} = \langle \Psi_A | el_A | \Psi_{A^*} \rangle,$$

where $\boldsymbol{l}_D$ and $\boldsymbol{l}_A$ are the position vectors of the electrons belonging to D and A, respectively.

$$\text{(24)} \qquad \beta_{\mathrm{C}} = \frac{1}{4\pi\varepsilon_0 n^2} \frac{1}{R_{DA}{}^3} |\mu_{D^* D}| |\mu_{AA^*}| \kappa_{D^* A}.$$

This equation not only forms a basis for describing the rate constant k_{EnT} but it also gives information about the influence of the ETDM interaction on the electronic states of D^* and A.

2`2. *Exciton splitting*. – We consider a pair of chromophores A_i and A_k at a distance R which is such that their interaction in the electronic ground state is negligibly small. We further assume that the overlap of the wave functions in the electronically excited states $A_i^* \ldots A_k$ and $A_i \ldots A_k^*$ between the neighbors (A_i^* and A_k) and (A_i and A_k^*) is negligible. This means that the "optical electrons" associated with the chromophoric units

preserve essentially their individual characteristic. This does, however, not necessarily mean that the interaction β_C between the electronically excited-state configurations $(A_i^* \ldots A_k)$ and $(A_i \ldots A_k^*)$ is so weak that the splitting of the corresponding states is negligible. The ETDM's μ_{A^*A} and μ_{AA^*} have the same value, hence, eq. (24) can be written as follows:

$$(25) \qquad \beta_C = \frac{1}{4\pi\varepsilon_0 n^2} \frac{|\mu_{AA^*}|^2}{R_{DA}{}^3} \kappa_{A^*A},$$

where κ_{A^*A} is defined by eq. (16). The wave function of the ground state and of the electronically excited states can be expressed as follows:

$$(26) \qquad \Psi_{A_i A_k} = \Psi_{A_i} \Psi_{A_k},$$

$$(27) \qquad \Psi_{A_i^* A_k} = \Psi_{A_i^*} \Psi_{A_k},$$

$$(28) \qquad \Psi_{A_i A_k^*} = \Psi_{A_i} \Psi_{A_k^*}.$$

We denote the energy of the electronic ground state $\Psi_{A_i A_k}$ as E_0 and that of the electronically excited states $\Psi_{A_i^* A_k}$ and $\Psi_{A_i A_k^*}$ in the absence of any interaction between them as E_1. In the presence of some interaction, as expressed by the perturbation H'_C, the excited state is more accurately described by means of a linear combination of the wave functions (27) and (28):

$$(29) \qquad \Phi(c_1, c_2) = c_1 \Psi_{A_i^* A_k} + c_2 \Psi_{A_i A_k^*}.$$

From this we find

$$(30) \qquad \langle \Phi(c_1, c_2) | H | \Phi(c_1, c_2) \rangle = \varepsilon \langle \Phi(c_1, c_2) | \Phi(c_1, c_2) \rangle,$$

where H is equal to $H_i + H_k + H'_C$. Evaluating this by keeping in mind that, according to the conditions mentioned above, the overlap integral $\langle \Psi_{A_i^* A_k} | \Psi_{A_i A_k^*} \rangle$ is zero, we obtain

$$(31) \qquad \begin{vmatrix} h_{11} - \varepsilon & h_{12} \\ h_{21} & h_{22} - \varepsilon \end{vmatrix} = 0$$

and

$$(32) \qquad \Phi_+ = \frac{1}{\sqrt{2}} \left(\Psi_{A_i^* A_k} + \Psi_{A_i A_k^*} \right),$$

$$(33) \qquad \Phi_- = \frac{1}{\sqrt{2}} \left(\Psi_{A_i^* A_k} - \Psi_{A_i A_k^*} \right).$$

The values of h_{11} and h_{22} are equal to E_1 while h_{12} and h_{21} are equal to β_C, eq. (25). This leads to

$$(34) \qquad \varepsilon_+ = E_1 + \beta_C, \qquad \varepsilon_- = E_1 - \beta_C.$$

Interchange of the molecular labels i, k indicates that Φ_+ is symmetric, while Φ_- is antisymmetric. The excitation is on both molecules i and k in both stationary states Φ_+
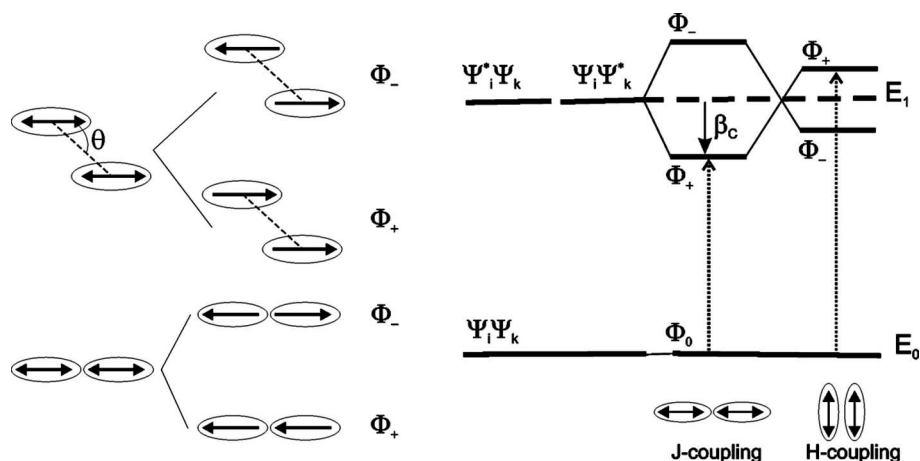
Fig. 7. – Phase relation and energy level diagram. Left: diagram showing the phase relation of the wave functions eqs. (32), (33) which describe the interaction caused by the ETDM between the electronically excited-state configurations $A_i^* \ldots A_k$ and $A_i \ldots A_k^*$. Right: energy level diagram showing the exciton splitting of two chrompophores caused by the interaction of the configurations due to the ETDM. This interaction naturally causes only a splitting of electronically excited states and has no consequences on the ground state. The different splitting of the excited-state levels for ETDM oriented in-line or parallel, as represented by means of double arrows, is due to the angle dependence of κ_{AA^*}. The allowed electronic transitions are indicated by the dotted arrows.

and Φ_-. The excitation is collective or delocalized. The node corresponding to the minus sign in Φ_- is an excitation node. At an excitation node, the relation between the ETDM of the respective molecular centers changes phase. We explain this in fig. 7 (left) for an arrangement of the ETDM with $\phi_{12} = 0$ and $\theta_1 = \theta_2$ which is frequently observed for dyes in nanochannels, as illustrated in fig. 3. Inserting these values into eq. (16) results in the simplified expression (35):

$$(35) \qquad\qquad \kappa_{AA^*} = 1 - 3\cos^2\theta.$$

The value of β_{C} is largest for in-line orientation and changes sign for parallel orientation. We illustrate this in the energy level diagram in fig. 7 (right). Situations with essentially in-line arrangement of the ETDM, lead to J-coupling, while those with essentially parallel arrangement lead to H-coupling. The corresponding arrangements of the chromophores are often named as J-aggregates and H-aggregates, respectively [15], names which are less meaningful in the present context.

According to eq. (35), the crossing of the Φ_+ and Φ_- levels occurs if $\cos^2(\theta)$ is equal to 0.333 which is the case if θ is equal to the magic angle of $54.7°$. The order of magnitude of the expected splitting $|2\beta_{\mathrm{C}}|$ can be estimated using the relation between the oscillator strength f of the electronic transition and the magnitude of the ETDM:

$$(36) \qquad\qquad f = \frac{8\pi c m_e}{3he^2}\bar{v}|\mu_{AA^*}|^2,$$

where e is the elementary charge, h is Plank's constant, m_e the electron mass, c the
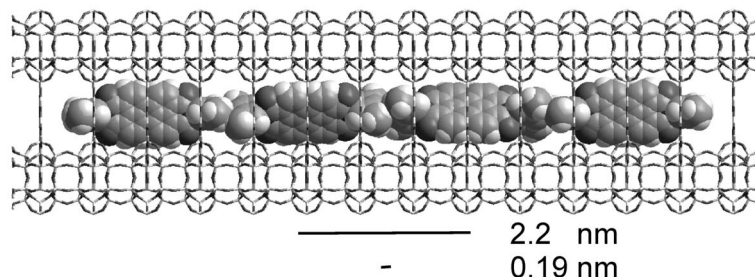
Fig. 8. – Comparison of the length of PR149 (2.2 nm) with the ETDM (0.19 nm), aligned in a zeolite L channel.

speed of light in vacuum and $\bar{\nu}$ the energy in cm^{-1} of the transition $A \rightarrow A^*$ [21, 22]. This equation is also useful for estimating the length of the ETDM. This is important because the validity of the dipole-dipole coupling theory depends on the condition that the distance between the ETDM of the two involved chromophores is large with respect to the length of the ETDM l_{μ^*}. Solving eq. (36) for μ_{A^*A}, dividing it by the elementary charge and inserting the constants leads to

$$(37) \qquad\qquad l_{\mu^*} = 3.036 \times 10^{-6} \, cm^{0.5} \sqrt{\frac{f}{\bar{\nu}}} \,.$$

From this equation we find, as an example, the length of the ETDM of an organic molecule with an oscillator strength of $f = 1$ absorbing at 500 nm to be 0.215 nm. This means that the distance between the molecules of interest in the zeolite L channels is in general large enough so that the dipole-dipole coupling approach can be considered as a good approximation. We illustrate this for PR149 (scheme in fig. 8) for which we calculate the length of the ETDM to be about 0.19 nm while the shortest distance between two molecules in the channels of zeolite L is about 2.2 nm.

Inserting eq. (36) in the expression for β_C, eq. (25) leads to eq. (38):

$$(38) \qquad\qquad \beta_C = \frac{3he^2}{32\pi^2 cm_e\varepsilon_0} \frac{f}{\bar{\nu}} \frac{\kappa_{A^*A}}{R_{DA}{}^3} \frac{1}{n^2} \,.$$

It is convenient to substitute the constant term by writing

$$(39) \qquad\qquad \beta_C = AD \frac{f}{\bar{\nu}} \frac{\kappa_{A^*A}}{R_{DA}{}^3} \frac{1}{n^2} \,.$$

The value of the constant AD is equal to $1.615 \times 10^{-18} \, m^2 \, cm^{-1}$ if we express β_C in cm^{-1}, which is convenient.

We discuss some consequences of this by using a perylene dye as example because these dyes have been used in different experiments [16, 23] and because they are well aligned parallel to the channel axis, which means that the angles ϕ_{12}, θ_1 and θ_2 are approximately zero, and because dyes with different types of subtituents R are know where R does not affect the electronic spectra of the molecules. The substituent R, however, determines the shortest distance between two chromophores at high packing which simplifies the discussion. This is useful for studying the dipole-dipole coupling
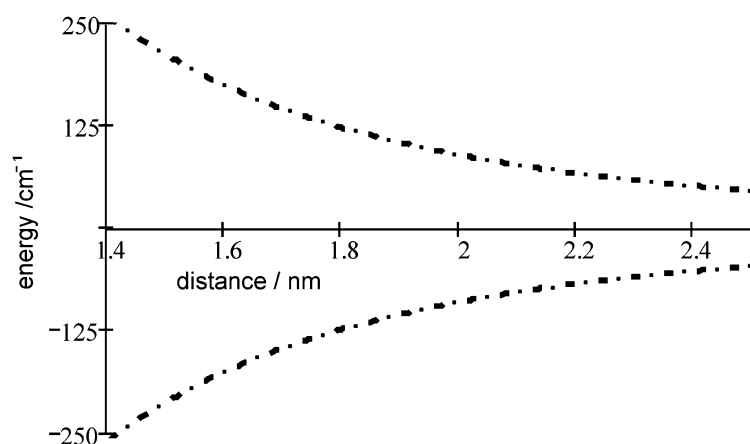
Fig. 9. – Exciton splitting of the stationary states Φ_- and the Φ_+ caused by the J-coupling as a function of the separation calculated for $f = 0.8$, $\bar{v} = 20000\,\mathrm{cm}^{-1}$ and $n = 1.45$.

strength. We show in fig. 9 the exciton splitting of the stationary Φ_- and the Φ_+ states caused by the J-coupling as a function of the separation.

The shortest high packing distance which can be realized for $R = \mathrm{CH}_3$ is in the order of 1.5 nm at which the level splitting of two interacting molecules is about $400\,\mathrm{cm}^{-1}$. It is about $100\,\mathrm{cm}^{-1}$ at 2.2 nm. Pc21 has an oscillator strength of about 1.4 which causes stronger J-coupling. Its ETDM is polarized along the channel axis. The absorption and the fluorescence spectra of Pc21 shown in fig. 10 illustrate nicely the consequences of the J-coupling [16]. The nicest demonstration of exciton coupling has been recently reported for pyronine loaded zeolite L for which correlated fluorescence microscopy, fluorescence lifetime and spectral imaging of single crystals were performed. At higher loading the molecules hinder themselves when entering the channels in a process which can be described as "traffic jam in nanochannels". This causes J-coupling in the region of the channel entrance [17].

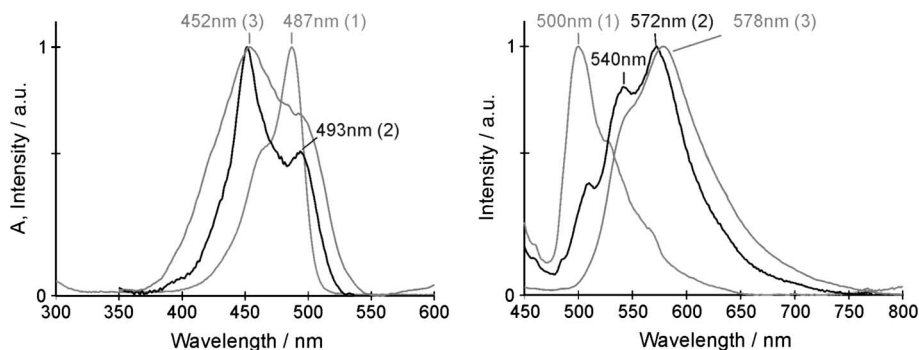Fig. 10. – Absorption, excitation and emission spectra of Pc21 scaled to 1 at the peak maxima. Left: absorption spectrum of Pc21 in 10^{-6} M solution (1), excitation spectra of Pc21-zeolite L at $p = 0.068$ (2, emission observed at 540 nm) and $p = 0.18$ (3, emission observed at 640 nm). Right: emission spectra of Pc21-zeolite L at $p = 0.045$ (1), at $p = 0.068$ (2) and $p = 0.18$ (3) [16].
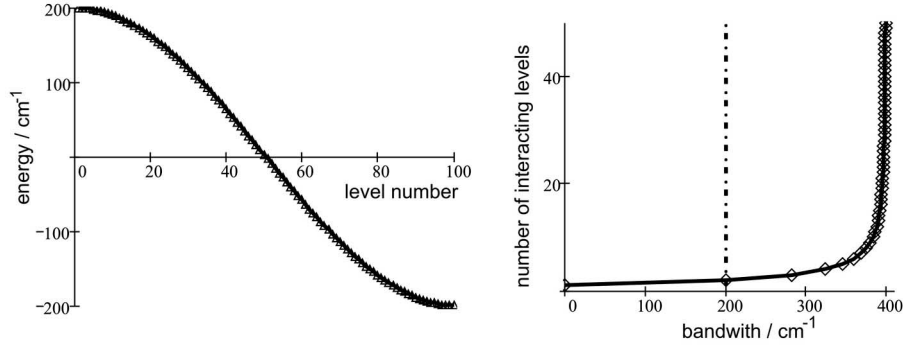
Fig. 11. – Energy levels and bandwidth, calculated for J-coupling with $\beta_C = 100\,\text{cm}^{-1}$. Left: energy levels of an exciton extended over 100 chromophores. Right: bandwidth for a varying number of interacting levels. The dash-dotted line corresponds to $N = 2$.

Interaction between two neighbours has been discussed, so far. The experimentally observed phenomena in high packing situations are in general expected to be due to interactions between more than two units. Generalization of the exciton splitting due to interaction of N chromophores is straightforward. It leads to eq. (40), where α denotes the energy in the absence of any interaction and j is equal to $1, 2, \ldots, N$.

$$(40) \qquad \varepsilon(j, N) = \alpha + 2\beta_C \cos\left(\frac{j}{N+1}\pi\right).$$

This means that N interacting chromophores generate N levels. This causes some broadening of the spectra; especially of the absorption spectra. The maximum splitting $\Delta E(N)$ caused is the difference between the level $\varepsilon(1, N)$ and $\varepsilon(N, N)$. We see from eq. (41) that it converges rapidly to the value of $4|\beta_C|$:

$$(41) \qquad \Delta E(N) = 2|\beta_C|\left(\cos\left(\frac{1}{N+1}\pi\right) - \cos\left(\frac{N}{N+1}\pi\right)\right).$$

We illustrate the contents of eqs. (40) and (41) in fig. 11 for $N = 100$ and $\beta_C = 100\,\text{cm}^{-1}$, while the value of α has been chosen to be equal 0. The consequences of the possibility to prepare densely loaded dye-nanochannel materials have only very scarcely been explored so far [16, 17].

3. – Energy transfer FRET

We consider the EnT transfer $D^*(0') + A(0) \rightarrow D(0) + A^*(2')$, which we can also express as $D^*(0')A(0) \rightarrow D(0)A^*(2')$. The rate constant for EnT between two selected levels which are in resonance is, according to eq. (17),

$$(42) \qquad k_{\text{EnT}(0',0;0,2')} = \frac{2\pi}{\hbar}\beta_{D^*A}{}^2\rho_{(0',0;0,2')},$$

where β_{D^*A} is equal to β_C. In order to find all transitions which take place between D^* and A, $D^*\ldots A \rightarrow D\ldots A^*$, we must sum over all states which are in resonance. We are

interested in condensed phase. Hence, rotational levels play no role. Denoting the states of the donor as (d', δ) and those of the acceptor as (α, a') the transfer rate constant can be expressed as follows:

$$(43) \qquad k_{\text{EnT}(d',\delta;\alpha,a')} = \frac{2\pi}{\hbar}\beta_{\text{C}}{}^2\rho_{(d',\delta;\alpha,a')}.$$

Since energy transfer can be very fast, it is not sufficient to consider only the lowest vibrational state of the donor. We must sum over all iso-energetic situations. This means that we must sum over all donor and acceptor states which are in resonance.

$$(44) \qquad k_{\text{EnT}} = \sum k_{\text{EnT}(d',\delta;\alpha,a')}.$$

There is no need to assume that the donor is in a thermally relaxed excited state. Energy transfer can often be so fast that there is no time left for establishing thermal equilibrium. This means that k_{EnT} can be time dependent. We do not want to take this explicitly into account but it is good to keep it in mind. It would in fact lead to a correction in the expression of the spectral overlap integral. Spectra in condensed phase are usually broadened due to solute solvent interactions and lattice vibrations. Hence, the initial (i) and the final (f) levels of $D^* \ldots A$ and $D \ldots A^*$ are broadened. We may therefore express the density of states ρ_E within a continuous energy range. We introduce the normalized functions $S_D(E_{D^*})$ and $S_A(E_A)$. The first expresses the probability that an excited molecule D^* emits photons of energy E_{D^*} and the second represents the probability that A absorbs photons of energy E_A.

$$(45) \qquad \int_{E_\gamma} S_\gamma(E_\gamma)\mathrm{d}E_\gamma = 1.$$

$S_D(E_{D^*})$ and $S_A(E_A)$ reflect the shape of the luminescence spectrum of D^* and of the absorption spectrum of A, respectively. The resonance condition, illustrated in fig. 12, can be expressed as follows:

$$(46) \qquad E_{D^*} = E^D_{0'0} + \varepsilon_{D^*} - \varepsilon_D,$$

$$(47) \qquad E_A = E^A_{0'0} + \varepsilon_{A^*} - \varepsilon_A,$$

$$(48) \qquad E_{\text{res}} = \int E_{D^*}\delta(E_{D^*} - E_A)\mathrm{d}E_{D^*}.$$

The rate constant for the EnT $D^* + A \rightarrow D + A^*$ is given as integral over the resonant energy range:

$$(49) \qquad k_{\text{EnT}} = \frac{2\pi}{\hbar}\int_{E_{D^*}}\int_{E_A}\beta_{\text{C}}{}^2 S_D(E_{D^*})S_A(E_A)\delta(E_{D^*} - E_A)\mathrm{d}E_{D^*}\mathrm{d}E_A.$$

Inserting β_{C} we get

$$(50) \qquad k_{\text{EnT}} = \frac{2\pi}{\hbar}\left(\frac{\kappa_{D^*A}}{4\pi\varepsilon_0 n^2 R_{DA}{}^3}\right)\int_{E_{D^*}}\int_{E_A}|\mu_{D^*D}|^2 S_D(E_{D^*})$$
$$\times |\mu_{AA^*}|^2 S_A(E_A)\delta(E_{D^*} - E_A)\mathrm{d}E_{D^*}\mathrm{d}E_A.$$
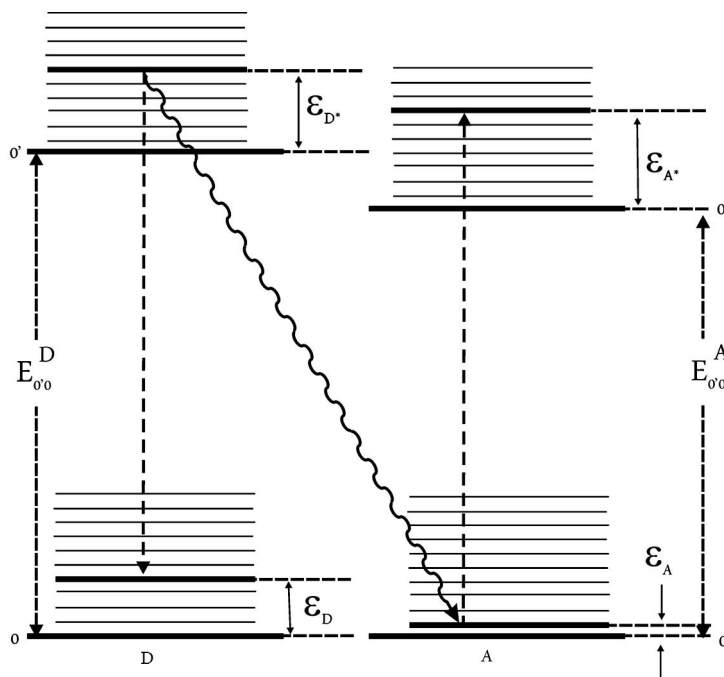
Fig. 12. – Energy levels of a donor D and an acceptor molecule A illustrating the conditions for resonance energy transfer in a more general way than in fig. 4.

An interesting way to evaluate this integral is using the Einstein coefficients A and B. The ETDM times the distribution functions can be substituted by the lifetime and the shape of the luminescence spectrum of the donor D^* and by the absorption spectrum of the acceptor A. Instead of integrating over the energy, we integrate over the frequency ν. Since $E = h\nu$, dE must be substituted by $h\,d\nu$. We also substitute the arguments E_{D^*} and E_A by ν_{D^*} and ν_A, respectively:

$$(51) \quad k_{\mathrm{EnT}} = \frac{1}{\hbar^2} \left(\frac{\kappa_{D^*A}}{4\pi\varepsilon_0 n^2 R_{DA}{}^3} \right)^2 \int_{\nu_{D^*}} \int_{\nu_A} |\mu_{D^*D}|^2 S_D(\nu_{D^*})$$

$$\times |\mu_{AA^*}|^2 S_A(\nu_A)\delta(\nu_{D^*} - \nu_A)\mathrm{d}\nu_{D^*}\mathrm{d}\nu_A.$$

The connection between the ETDM and the Einstein coefficient for induced absorption or emission, B_{D^*D}, and that for spontaneous emission, A_{D^*D}, can be expressed as follows:

$$(52) \qquad\qquad B_{D^*D} = \frac{2\pi}{3\hbar^2} \frac{1}{4\pi\varepsilon_0} \frac{1}{n^2} (\mu_{D^*D})^2,$$

$$(53) \qquad\qquad A_{D^*D} = 8\pi \frac{h\nu_{D^*}{}^3}{c_0{}^3} n^3 B_{D^*D},$$

where c_0 is the vacuum speed of light. These two relations are used, after some lengthy reasoning which we skip, to turn the rather complicated expression for the energy transfer

rate constant (51) into the practical form (54) which was derived by Th. Förster [4].

$$(54) \qquad k_{\mathrm{EnT}} = TF \cdot c_0 \frac{\kappa_{D^*A}{}^2}{n^4 R_{DA}{}^6} \frac{1}{\tau_{0,D^*}} \int_\nu S_D(\nu) \frac{\varepsilon_A(\nu)}{\nu^4} \mathrm{d}\nu.$$

The value of the Theodor Förster constant TF is given by

$$(55) \qquad TF = \frac{9000 \ln(10)}{128 \pi^5 N_L} \quad \text{or} \quad TF = 8.785 \times 10^{-25} \, \text{mol}.$$

We often prefer to record spectra in wave numbers (cm^{-1}), using the relation between frequency and wave number:

$$(56) \qquad \nu = \bar{\nu} c_0.$$

The dimension of $S(\nu)$ is equal to that of ν. Hence, expressing the spectral overlap integral in wave numbers and using $\tau_{D^*} = \phi_{D^*} \tau_{0,D^*}$, where ϕ_{D^*} is the luminescence quantum yield of D^* in the absence of energy transfer, we get

$$(57) \qquad k_{\mathrm{EnT}} = TF \frac{\kappa_{D^*A}{}^2}{n^4 R_{DA}{}^6} \frac{\phi_{D^*}}{\tau_{D^*}} \int_{\bar{\nu}} S_D(\bar{\nu}) \frac{\varepsilon_A(\bar{\nu})}{\bar{\nu}^4} \mathrm{d}\bar{\nu}.$$

This equation leads to the definition of the spectral overlap integral which is usually abbreviated with the symbol J:

$$(58) \qquad J_{\bar{\nu}D^*A} = \int_{\bar{\nu}} S_D(\bar{\nu}) \frac{\varepsilon_A(\bar{\nu})}{\bar{\nu}^4} \mathrm{d}\bar{\nu}.$$

The dimension of J in formula (58) is $[\mathrm{cm}^3\,\mathrm{M}^{-1}]$. The molar extinction coefficient $\varepsilon_A(\bar{\nu})$ is usually expressed in $\mathrm{M}^{-1}\,\mathrm{cm}^{-1}$ where $[\mathrm{M}] = [\mathrm{mol}\,\mathrm{L}^{-1}]$. The other dimensions are: $[\tau_{D^*}] = [\mathrm{ns}]$, $[R_{DA}] = [\mathrm{\AA}]$, and $[N_L] = [\mathrm{mol}^{-1}]$. With this, the dimension of the energy transfer rate constant is $[\mathrm{ns}^{-1}]$. This is convenient for a majority of applications.

$$(59) \qquad [k_{\mathrm{EnT}}] = \frac{1}{\mathrm{mol}^{-1}} \frac{1}{\mathrm{\AA}^6} \frac{1}{\mathrm{ns}} \frac{\mathrm{cm}^3}{\mathrm{mol}\cdot\mathrm{L}^{-1}} 10^{51} = \mathrm{ns}^{-1}.$$

Using instead of this $[J] = [\mathrm{cm}^6\,\mathrm{mol}^{-1}]$ the rate constant k_{EnT} is

$$(60) \qquad k_{\mathrm{EnT}} = TF^* 10^{-3} \frac{\kappa_{D^*A}{}^2}{n^4 R_{DA}{}^6} \frac{\phi_{D^*}}{\tau_{D^*}} J_{\bar{\nu}D^*A}.$$

In the next sections we address some consequences of the important equation (57) for the rate constant of electronic excitation energy transfer.

The efficiency of FRET depends on the inverse sixth power of the intermolecular separation making it useful over distances in the range of $1.5\,\mathrm{nm}$ to $10\,\mathrm{nm}$. Thus, FRET is an important technique for investigating a variety of phenomena that produce changes in molecular proximity. A condition for FRET is that the absorption spectrum of the acceptor overlaps with the fluorescence spectrum of the donor. We illustrate this spectral overlap in fig. 13 for the molecules Py and Ox.
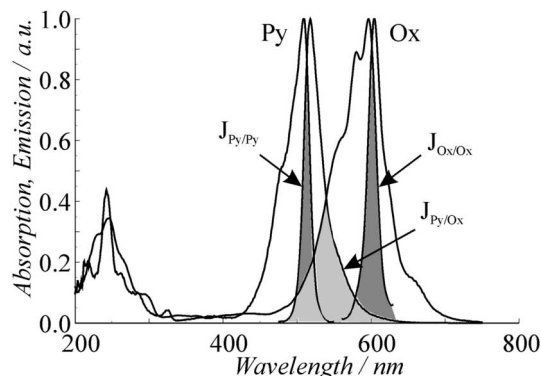
Fig. 13. – Absorption and fluorescence spectra of two fluorescent dyes, Py and Ox, scaled to the same height at the maximum. The picture shows three spectral overlap regions: that of the absorption and fluorescence of the individual dyes ($J_{\mathrm{Py/Py}}$ and $J_{\mathrm{Ox/Ox}}$) and that of the fluorescence spectrum of Py with the absorption spectrum of Ox ($J_{\mathrm{Py/Ox}}$).

3˙1. Förster energy transfer radius. – A special situation occurs at a donor to acceptor distance at which the EnT rate is equal to the luminescence decay. To analyze this situation for an isotropic three-dimensional system, we write the rate of luminescence of an excited molecule and the EnT rate to an acceptor (eqs. (61) and (62)):

$$(61) \qquad \text{Luminescence rate of } D^*: \left(\frac{\mathrm{d}\rho_{D^*}}{\mathrm{d}t}\right)_{\text{fluorescence of } D^*} = -\frac{1}{\tau_{D^*}}\rho_{D^*},$$

$$(62) \qquad \text{Energy transfer rate:} \left(\frac{\mathrm{d}\rho_{D^*}}{\mathrm{d}t}\right)_{\text{EnT}} = -k_{\text{EnT}}\rho_{D^*}.$$

The rate at which D^* emits light is equal to the rate at which it transfers its excitation energy to A at a specific $D^*\ldots A$ distance:

$$(63) \qquad \frac{1}{\tau_{D^*}} = k_{\text{EnT}}.$$

We name the donor to acceptor distance at which (63) holds, critical distance or Förster radius R_0. Inserting (63) in (57) and solving for R_0 results in

$$(64) \qquad R_0{}^6 = TF\frac{\kappa_{D^*A}{}^2}{n^4}\phi_{D^*}J_{\bar{\nu}D^*A}.$$

From this we find the Förster radius R_0 for electronic excitation energy transfer.

$$(65) \qquad R_0 = \sqrt[6]{TF\frac{\kappa_{D^*A}{}^2}{n^4}\phi_{D^*}J_{\bar{\nu}D^*A}}.$$

R_0 is equal to the donor-acceptor distance at which the probability for energy transfer is 50%. Substituting (65) in (57) the very useful formula (66) is obtained. It allows

determining the energy-transfer-constant as a function of distance, provided that we know the spectral overlap and the natural luminescence decay time of the donor.

$$(66) \qquad k_{\text{EnT}} = \frac{1}{\tau_{D^*}} \left(\frac{R_0}{R} \right)^6 .$$

3'2. *Probability for energy transfer*. – We now consider the distance dependence of the probability P for energy transfer. For this we write

$$(67) \qquad P = \frac{\left(\frac{\text{d}\rho}{\text{d}t} \right)_{\text{EnT}}}{\left(\frac{\text{d}\rho}{\text{d}t} \right)_{\text{fluorescence}} + \left(\frac{\text{d}\rho}{\text{d}t} \right)_{\text{EnT}}} .$$

Canceling $\left(\frac{\text{d}\rho}{\text{d}t} \right)_{\text{EnT}}$ and using (61) and (62) gives

$$(68) \qquad P = \frac{1}{\frac{1}{\tau_{D^*} k_{\text{EnT}}} + 1} .$$

Inserting into (66), the probability for EnT can be expressed as follows:

$$(69) \qquad P = \frac{1}{1 + (R/R_0)^6} .$$

This equation illustrates a way to measure distances in macromolecules or biological systems, by simply considering the energy transfer efficiency between a donor and an acceptor attached to the object of investigation. It is only valid if the involved chromophores are embedded in a three-dimensional isotropic medium [24]. For other conditions it can be expressed as follows:

$$(70) \qquad P = \frac{1}{1 + (R/R_0)^\alpha} ,$$

where the exponent α reflects the dimensionality of the system. It is equal to six for three-dimensional systems, equal to four for two-dimensional systems and becomes equal to two in the one-dimensional case. We observed in dye loaded zeolite materials α values of 2 which means quasi–one-dimensional behaviour [16].

3'3. *Selection rules*. – There are no strict selection rules for Förster energy transfer. We can, nevertheless, get a good idea by considering the following proportionality:

$$(57a) \qquad k_{\text{EnT}} \propto \frac{\phi_{D^*}}{\tau_{D^*}} \int_{\bar{\nu}} S_D(\bar{\nu}) \frac{\varepsilon_A(\bar{\nu})}{\bar{\nu}^4} \text{d}\bar{\nu}.$$

This means that the energy transfer rate constant depends on the extinction coefficient of the acceptor. If a forbidden transition of the acceptor is involved, the energy transfer rate is small. If the natural lifetime of the donor is large, the rate constant is scaled,

TABLE II. – *Spectral overlap, Förster radius for two values of $\kappa_{D^*A}{}^2$ and EnT rate constant for molecules in zeolite L at room temperature.*

Dyes Donor/acceptor	Spectral overlap (J/cm^3 M^{-1})	$\kappa_{D^*A}{}^2$	R_0 (Å)	Fluorescence lifetime (ns)	k_{EnT} (ps^{-1})	
					$R = R_0$	$R = 1.5\,\mathrm{nm}$
Ox/Ox	4.4×10^{-13}	2/3	64	3.2	3.1×10^{-4}	1.9
		4	86			11
Py/Py	1.1×10^{-13}	2/3	51	3	3.3×10^{-4}	0.5
			68			2.9
Py/Ox	2.3×10^{-13}	4	57	3	3.3×10^{-4}	1.0
			77			6.0
Ox1/Ox1	4.9×10^{-13}	2/3	73	3.2	3.1×10^{-4}	4.1
		4	98			24

correspondingly. Hence, the following reactions are examples of allowed Förster energy transfer processes [24]:

$$
\begin{aligned}
{}^1D^* + {}^1A &\rightarrow {}^1D + {}^1A^*, \\
{}^1D^* + {}^3A^* &\rightarrow {}^1D + {}^3A^{**}, \\
{}^3D^* + {}^1A &\rightarrow {}^1D + {}^1A^*, \\
{}^3D^* + {}^3A^* &\rightarrow {}^1D + {}^3A^{**}.
\end{aligned}
\tag{71}
$$
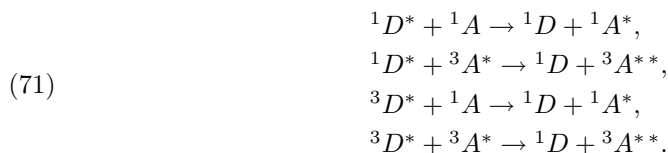
We note that the rate constant decreases with increasing luminescence lifetime of the donor. The process can nevertheless be very efficient because the system gains time for this process to occur but has also much time for other relaxation processes. Energy transfer from a ruthenium stopcock to an organic dye inside the channels of zeolite L is a nice example for a ${}^3D^* + {}^1A \rightarrow {}^1D + {}^1A^*$ energy transfer [25].

3 4. *Examples for spectral overlap and Förster radius.* – The spectral overlap between the emission of an electronically excited D^* and a molecule A is defined in eq. (58). Knowing the spectral overlap integral, we can calculate the Förster radius R_0 according to (65). Knowing the Förster radius and the natural fluorescence lifetime of the donor we can calculate the energy transfer rate constant according to (66). We report some data in table II calculated for a refractive index of 1.33 for two different values of $\kappa_{D^*A}{}^2$ and two distances R for some selected molecules. From this we see that rate constants in the order of $10^{12}\,\mathrm{s}^{-1}$ have to be considered as being quite common and that in favorable cases rate constants in the order of a few times $10^{13}\,\mathrm{s}^{-1}$ should be possible.

The spectra and hence the spectral overlap J of the molecules depend often considerably on the environment and on the temperature. We illustrate this in fig. 14 for Ox and Py in zeolite L. In these two cases J changes only slightly despite of the increasing resolution of the vibrational structure with decreasing temperature [26]. This can, however, not be generalized and should always be checked for the specific conditions of interest.
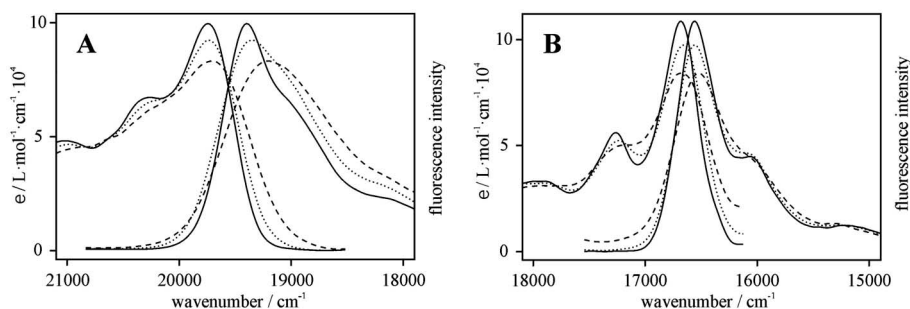
Fig. 14. – Fluorescence and excitation spectra of dye loaded zeolite L at different temperatures. A) Py-zeolite L and B) Ox-zeolite L at $80\,\mathrm{K}$ (solid), $193\,\mathrm{K}$ (dotted) and $293\,\mathrm{K}$ (dashed). The fluorescence spectra have been scaled to the same height as the corresponding excitation spectra [26].

4. – Luminescence intensity dynamics

Consider a set of non-interacting molecules A. If one of them is excited to become A^*, energy transfer to a neighbouring A can take place. This process is repeated until the excitation energy is captured by a trap or lost, *e.g.*, by luminescence or by radiationless decay, as illustrated in fig. 15.

As a result electronic excitation energy is transported in space. An important quality of this energy migration is that it cannot be observed by just measuring the luminescence decay of A^*, as we shall discuss now. We assume that a molecule A is excited electronically at time $t = 0$ by absorption of a photon. The probability that A is in the excited state at time t is $\rho_A(t)$. At $t = 0$ we have: $\rho_A(0) = 1$. The decay of the excitation probability is

$$(72) \qquad \frac{\mathrm{d}\rho_A}{\mathrm{d}t} = -\frac{1}{\tau}\rho_A,$$

where τ is the decay time (mean lifetime). Solving this equation gives

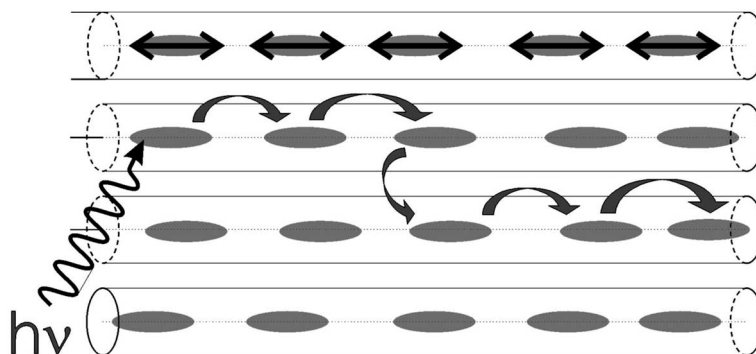$$(73) \qquad \rho_A(t) = \rho_A(0)e^{-t/\tau}.$$

Fig. 15. – Migration of electronic excitation energy among similar molecules.

τ_0 is the natural lifetime and corresponds to the lifetime in the absence of other relaxation processes. If all decay processes which result in deactivation of A^* to the ground state are of first order with the decay constants k_i, we write

$$(74) \qquad\qquad \tau = \frac{1}{\sum_i k_i} \quad \text{and} \quad \tau_0 = \frac{1}{k_0}.$$

The luminescence yield ϕ_L can be expressed as follows:

$$(75) \qquad\qquad \phi_L = \frac{1}{\tau_0} \int_0^\infty \rho_A(t)\mathrm{d}t = \frac{\tau}{\tau_0}.$$

We number alike molecules A with the indices k and j. If there is a possibility for a radiationless transition $A_k^* \to A_j$ to occur, then the decrease of A_k^* is proportional to the probability ρ_{Ak} that A_k is in the excited state. There is an equal increase of the excitation probability ρ_{Aj} of the molecule A_j. Considering these processes between all molecules:

$$(76) \qquad\qquad \frac{\mathrm{d}\rho_{A_k}}{\mathrm{d}t} = \sum_j \overline{F}_{kj}(\rho_{A_j} - \rho_{A_k}) - \frac{1}{\tau}\rho_{A_k},$$

where $\overline{F}_{kj}$ is the mean rate constant for the radiationless transfer $A_k^* \to A_j$. Equation (76) can be written in this form, because the mean rate constants for a transfer $A_j^* \to A_k$ has the same value, since we are studying alike molecules, which means: $\overline{F}_{kj} = \overline{F}_{jk}$. This holds because emission and energy transfer take place in parallel (at the same time). This formulation is different from the mechanism of self-absorption and re-emission where the processes are consecutive. This means that the decay of excitation probability $\frac{1}{\tau}\rho_{A_k}(t)$ is accompanied by a balancing out of the excitation probability among the individual molecules. In order to describe not only one molecule A_k^* interacting with molecules A_j but the behavior of an ensemble we must sum over all cases:

$$(77) \qquad\qquad \sum_k \frac{\mathrm{d}\rho_{A_k}}{\mathrm{d}t} = \sum_k \left(\sum_j \overline{F}_{kj}(\rho_{A_j} - \rho_{A_k}) - \frac{1}{\tau}\rho_{A_k} \right).$$

In this equation the double sum cancels because $\overline{F}_{kj} = \overline{F}_{jk}$ holds:

$$(78) \qquad\qquad \sum_k \left(\sum_j \overline{F}_{kj}(\rho_{A_j} - \rho_{A_k}) \right) = 0.$$

From this, we find

$$(79) \qquad\qquad \sum_k \frac{\mathrm{d}\rho_{A_k}}{\mathrm{d}t} = -\frac{1}{\tau} \sum_k \rho_{A_k}.$$

Inserting $\rho_{A_k(t)}$ from eq. (73) leads to the following expression for the luminescence intensity which describes the situation after excitation of an ensemble of molecules:

$$(80) \qquad \sum_k \frac{d\rho_{A_k}}{dt} = -\frac{1}{\tau} \sum_k \rho_{A_k}(0) e^{-t/\tau} = -\frac{1}{\tau} e^{-t/\tau} \sum_k \rho_{A_k}(0).$$

Solving this differential equation we find that the sum of the excitation probabilities for the individual molecules is

$$(81) \qquad \sum_k \rho_{A_k}(t) = e^{-t/\tau} \sum_k \rho_{A_k}(0).$$

A more familiar way to write this equation is to express the excitation probability of A in terms of concentrations denoted as $[A^*]$:

$$(82) \qquad [A^*](t) = [A^*]_0 e^{-t/\tau}.$$

This means that in a homogeneous system on average the decay of luminescence of the ensemble is not affected by energy migration [4]. Hence, energy migration is not observed in a simple luminescence decay measurement. How can migration of excitation energy be observed? There are several possibilities. One of them is based on the fact that, under many conditions, excitation energy migration causes a change of the polarization of the emitted light. This can be observed in stationary and in time-resolved luminescence experiments [27, 28]. Another possibility is to add luminescent traps at well-defined positions in space [16] or to observe time and space resolved luminescence of an optically anisotropic material [16, 17, 28, 29].

4'1. *3D Systems of randomly mixed donor and acceptor molecules.* – We assume that N_D donor molecules D and N_{ac} acceptor molecules A are randomly distributed in a large volume, so that effects due to the border of the rigid system can be neglected. The molecules D and A are assumed to be at fixed positions. This means that they cannot move. A is assumed to absorb light at lower energy than D, so that energy transfer can occur from D^* to A but not in the reverse direction. This situation is schematically shown in the scheme of fig. 16.

We now discuss the decrease of the excitation probability of the donor. Any acceptor molecule A_i, at distance R_i from D^*, gives an additional channel for relaxation, the rate constant of which is $k_{EnT}(i)$:

$$(83) \qquad k_{EnT}(i) = \frac{1}{\tau_{D^*}} \left(\frac{R_0}{R_i} \right)^6.$$

The same is true for energy transfer not only to A_i but to any of the N_{ac} acceptor molecules. From this we find that the decrease of excitation probability of D^* can be expressed as follows:

$$(84) \qquad -\frac{d\rho_{D^*}}{dt} = (k_F + k_{IC})\rho_{D^*} + \left(\sum_{i=1}^{N_{ac}} k_{EnT}(i) \right) \rho_{D^*},$$

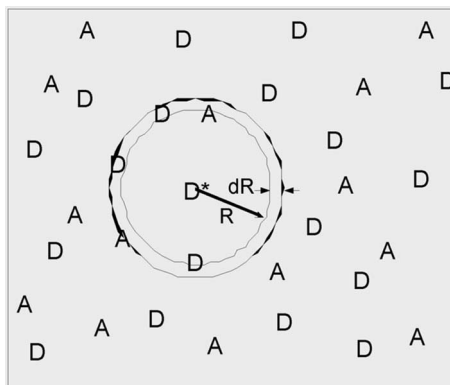$$(85) \qquad (k_F + k_{IC}) = \frac{1}{\tau_{D^*}}.$$

Fig. 16. – Randomly distributed donors D and acceptors A.

This means that we have $N_{ac} + 1$ independent deactivation channels

$$(86) \qquad \rho_{D^*} = \exp\left[-\left((k_F + k_{IC}) + \sum_{i=1}^{N_{ac}} k_{\text{EnT}}(i)\right) t\right]$$

and that the excitation probability of D^* decays exponentially. This can also be expressed as follows:

$$(87) \qquad (k_F + k_{IC}) + \sum_{i=1}^{N_{ac}} k_{\text{EnT}}(i) = \frac{1}{\tau_{D^*}} + \frac{1}{\tau_{D^*}} \sum_{i=1}^{N_{ac}} \left(\frac{R_0}{R_i}\right)^6.$$

We insert this in (86) and obtain

$$(88) \qquad \rho_{D^*} = e^{-\frac{t}{\tau_{D^*}}} \prod_{i=1}^{N_{ac}} \exp\left[-\left(\frac{R_0}{R_i}\right)^6 \frac{t}{\tau_{D^*}}\right].$$

We do not consider the decay of a single molecule D^* but that of a large number of statistically distributed molecules which have acceptors at statistically distributed distances R_i. $P(R_i)\mathrm{d}R_i$ is the probability that a given acceptor A_i is located in the environment of an electronically excited D^* at distance between R_i and $R_i + \mathrm{d}R_i$. Then the decrease of the mean excitation energy $\langle \rho_{D^*}(t) \rangle$ is

$$(89) \qquad \langle \rho_{D^*}(t) \rangle = e^{-\frac{t}{\tau_{D^*}}} \prod_{i=1}^{N_{ac}} \int_0^{R_V} \exp\left[-\left(\frac{R_0}{R_i}\right)^6 \frac{t}{\tau_{D^*}}\right] P(R_i)\mathrm{d}R_i.$$

It is convenient to write this equation as the product of the exponential, describing the fluorescence decay of the D^* in the absence of acceptors multiplied by the modification $G_D(t)$ of the decay caused by energy transfer.

$$(90) \qquad \langle \rho_{D^*}(t) \rangle = e^{-\frac{t}{\tau_{D^*}}} G_D(t),$$

$$(91) \qquad V = \frac{4\pi}{3} R_V{}^3.$$

Evaluation of the distribution function $G_D(t)$ for uniform statistical distribution of D and A in the three-dimensional space leads to

$$(92) \qquad G_D(t) = e^{-\sqrt{\pi}N_{\mathrm{ac}}(\frac{R_0}{R_V})^3\sqrt{\frac{t}{\tau_{D*}}}}.$$

The concentration of acceptor molecules in a spherical vessel of radius R_V in [mol/L] is

$$(93) \qquad c_{\mathrm{ac}} = \frac{N_{\mathrm{ac}}}{N_L}\left(\frac{4\pi}{3}R_V^3\right)^{-1}.$$

Using the definition

$$(94) \qquad 2\gamma = \sqrt{\pi}N_{\mathrm{ac}}\left(\frac{R_0}{R_V}\right)^3 \quad \text{or} \quad 2\gamma = \sqrt{\pi}c_{\mathrm{ac}}N_L\frac{4\pi}{3}R_0{}^3,$$

we obtain

$$(95) \qquad G_D(t) = e^{-2\gamma(\frac{t}{\tau_{D*}})^{1/2}}.$$

$4\dot{}2.$ *Lower-dimensionality systems.* – Lower dimensionality is expected and has also been observed in dye loaded zeolite L materials. Equation (95) can be extended, so that it applies for any dimensionality between 3 and one by introducing a parameter δ; eq. (96). δ is equal to $1/2$ in 3D systems. It becomes smaller as the dimensionality decreases: $1/3$ for 2D and $1/6$ for 1D systems [30].

$$(96) \qquad G_D(t) = e^{-2\gamma(\frac{t}{\tau_{D*}})^{\delta}}.$$

We define the critical concentration c_0 of acceptor molecules for a situation where γ is equal to one. This means that the critical concentration of acceptor molecules is represented by

$$(97) \qquad c_0 = \frac{\alpha}{N_L}\left(\frac{4\pi}{3}R_0{}^3\right)^{-1},$$

where α is a parameter that depends on the relative distribution of the ETDM. It is equal to $2/\sqrt{\pi}$ for random arrangement but can also be smaller or larger, depending on the situation. Hence, γ can be expressed as the ratio between the actual concentration of acceptor molecules and the critical concentration c_0:

$$(98) \qquad \gamma = \frac{c_{\mathrm{ac}}}{c_0}.$$

We wonder about the intensity of the emission of the donor at constant donor but varying acceptor concentration, expressed by means of the parameter γ. This can be done by investigating the fluorescence yield as a function of γ, for otherwise constant conditions. The fluorescence yield ϕ_{D*} of the donor is proportional to the integral over the whole time range from $t = 0$ to $t = \infty$, multiplied with the proportionality constant C. We compare
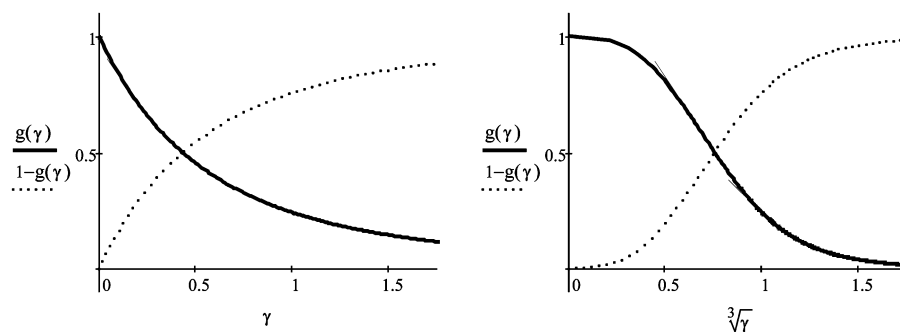
Fig. 17. – Plot of the ratio of the fluorescence quantum yield ratio $g(\gamma)$ *vs.* γ (left) and *vs.* $\sqrt[3]{\gamma}$ (right). We see on the left that the fluorescence quantum yield of the donor (solid line) decreases fast, while that of the acceptor (dashed line) increases accordingly.

in a 3D system ϕ_{D^*} with the luminescence yield in the absence of acceptors ϕ_{0,D^*}.

$$(99) \qquad \phi_{D^*} = c \int_0^\infty e^{-\frac{t}{\tau_{D^*}} - 2\gamma\sqrt{\frac{t}{\tau_{D^*}}}} \, \mathrm{d}t,$$

$$(100) \qquad \phi_{0,D^*} = c \int_0^\infty e^{-\frac{t}{\tau_{D^*}}} \, \mathrm{d}t = C\tau_{D^*},$$

$$(101) \qquad \frac{\phi_{D^*}}{\phi_{0,D^*}}(\gamma) = \frac{1}{\tau_{D^*}} \int_0^\infty e^{-\frac{t}{\tau_{D^*}} - 2\gamma\sqrt{\frac{t}{\tau_{D^*}}}} \, \mathrm{d}t.$$

Evaluating and using the abbreviation

$$(102) \qquad g(\gamma) = \frac{\phi_{D^*}}{\phi_{0,D^*}}(\gamma),$$

gives

$$(103) \qquad g(\gamma) = 1 - \gamma\sqrt{\pi}\exp[\gamma^2](1 - \mathrm{erf}(\gamma)).$$

The behavior of this quantum yield ratio is illustrated in fig. 17 where we plot $g(\gamma)$ *vs.* γ and *vs.* $\sqrt[3]{\gamma}$. We see that $g(\gamma)$ is proportional to the donor acceptor distance R. It is therefore not surprising that the plot shown on the right side of fig. 17 resembles the behavior of the energy transfer probability P, eq. (70), *vs.* distance.

Numerical methods are needed to describe more complex situations. Markow chain [9] and Monte Carlo methods [29] have been used by us to design and understand supramolecularly organized systems. An example is shown in fig. 18 where we present data of an antenna material.

Antenna systems are supramolecular arrangements in which electronic excitation of molecules occurs in a given volume and in which the electronic excitation energy is then transported by a radiationless process (near-field interactions) to a well-defined location. Sequential insertion of dyes in channels has been shown to be an excellent tool for preparing such systems [13, 16]. Figure 18A shows a schematic representation of an individual crystal of an antenna material. The crystal is filled with donor molecules in the middle, while the channel ends are occupied by acceptors. Energy is transported in two directions towards the channel ends; we therefore call this material *bidirectional*
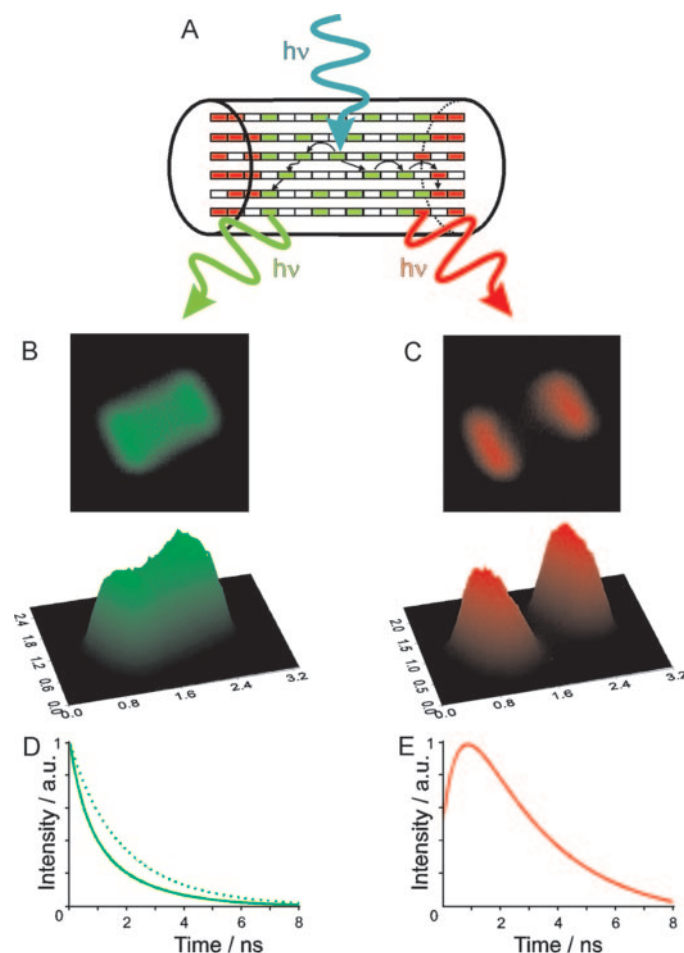
Fig. 18. – (Colour on-line) Fluorescence behaviour of an Ox,Py-zeolite L antenna. (A) Scheme of an antenna crystal and processes taking place upon excitation of a donor molecule: absorption of incident light, energy migration from an excited donor molecule to a neighboring unexcited one and trapping by an acceptor (black arrows), fluorescence of both donor and acceptor. (B) Confocal microscopy images of an antenna crystal upon selective excitation of the donor and observation through an appropriate filter. (C) Confocal microscopy images upon selective excitation of the acceptor. (D) and (E) Time-resolved intensity dynamics of the donor (D) and the acceptor (E) upon selective excitation of the donor. (D) Donor fluorescence dynamics in the absence (dotted) and in the presence (solid) of acceptors. The faster decay in the presence of acceptors indicates energy transfer taking place; (E) acceptor intensity dynamics. The rise of intensity reflects the "pumping" of acceptors through energy transfer [29].

antenna. If one of the green dyes is electronically excited, the excitation energy can travel randomly, until it is lost by spontaneous emission or captured by one of the red acceptors and then released by them as fluorescence. The confocal microscopy images of this material show nicely that the dyes are really situated as proposed by the schematic representation. We observe the green donor fluorescence in the middle part of the crystal upon selective excitation of the donor and applying an optical filter. Selectively exciting acceptors results in their red fluorescence at both crystal ends; fig. 18 B,C.
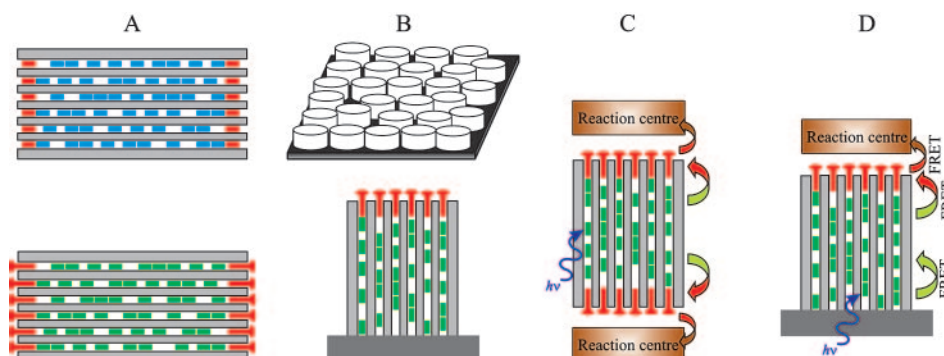
Fig. 19. – (Colour on-line) Representation of materials that have been successfully prepared fulfilling the criteria of different stages of supramolecular organisation. The length of the cylindrically shaped crystals is in the order of 50 nm up to a few hundred nm. A) Antenna materials are obtained by the consecutive insertion of different dye molecules. Bidirectional stopcock-plugged antenna materials are obtained by modifying the channel entrances with specific stopcock molecules [32]. B) Oriented monolayers of standing zeolite L crystals on a substrate (top) [33]. C and D) Interfacing antenna crystals to a reaction centre via stopcock molecules. Bidirectional (C) and monodirectional (D) electronic excitation energy transport materials connected to a photoelectronic or photochemical reaction centre. The excitation energy from the dyes in the channels (green rectangles) is transported via FRET to the stopcock molecules (red) located at the entrances. From there, the electronic excitation energy is transferred radiationlessly by near-field interaction (FRET) to a reaction centre.

Time-resolved investigations upon selective excitation of the donors show the behavior one would expect for Förster energy transfer. The donor intensity dynamics is shown in fig. 18D. The intensity decay in the presence of acceptors is faster (solid line) than the decay in the absence of acceptors (dotted line), as the energy transfer is an additional process depopulating the excited state of the donor. The intensity dynamics of the acceptors is shown in fig. 18E. It rises first before it starts to decay. The reason is that the acceptors are not excited directly but are "pumped" to the excited state via energy transfer. The more efficient the energy transfer, the faster is the rise, which is often difficult to be observed for molecules with a luminescence lifetime of only a few ns. This rise has been very nicely observed in the antenna materials [29] and also in mixed dye materials [31].

5. – Conclusions

The essential theoretical reasoning that has been used for developing and understanding nanochannel based antenna materials for capturing and transporting electronic excitation energy is based on ETDM interaction. The consequences are quasi-one-dimensional electronic excitation energy transport and J-coupling phenomena. A fascinating result of Försters theory [4, 5] and of Davydov's theory [14] is that both lead to simple equations useful for understanding complex phenomena. While it is possible to derive the Förster equations in a more general and theoretically more elegant way, we find that the semi-intuitive approach used by Förster, which we have followed here, leads to a good physical understanding of what is going on and hence helps to invent experiments which bring the formulas to life. Excitation energy migration has been described as hopping process. This is very useful and we intend to apply it also for the more complex materials under study, illustrated in fig. 19C and D and explained in more detail

in ref. [16]. The stopcock principle allows communication of dyes inside the channels with external species like a molecule, a polymer matrix, a semiconductor, a quantum sized particle, a molecular- or a nano-magnet, and a biochemical or a biological object. Electronic excitation energy transfer in such materials can be extremely fast because of their low dimensionality. We do not yet know much about the coherence length of the J-coupling but we would not be astonished if considerable coherent length could be realized. We wonder to what extent a hopping mechanism remains an adequate description of the process in such systems as the coupling strength can be larger than $100 \, \text{cm}^{-1}$. Precise time, space and spectrally resolved experiments on well-selected single crystals of about $1000 \, \text{nm}$ length will be needed in order to get the necessary experimental information. The systems are so versatile that fascinating results are to be expected.

REFERENCES

[1] LEVINE R. D. and BERNSTEIN R. B., *Molecular Reaction Dynamics* (Oxford University Press, NY) 1974.

[2] MAY V. and KÜHN O., *Charge and Energy Transfer Dynamics in Molecular Systems* (Wiley-VCH, Berlin) 2004, 2nd edition.

[3] a) ANDREWS D. L. and DEMIDOV A. A., *Resonance Energy Transfer* (John Wiley & Sons, NY) 1999; b) SCHOLES G. D., CURUTCHET C., MENNUCCI B., CAMMI R. and TOMASI J., *J. Phys. Chem. B*, **111** (2007) 6978; c) WANG X. F. and HERMAN B., *Fluorescence Imaging Spectroscopy and Microscopy* (John Wiley & Sons, NY) 1996; d) RITZ T., DAMJANOVIČ A. and SCHULTEN K., *ChemPhysChem*, **3** (2002) 243.

[4] a) FÖRSTER TH., *Ann. Phys. (Leipzig)*, **2** (1948) 55; b) *Fluoreszenz Organischer Verbindungen* (Vandenboeck & Ruprecht, Göttingen) 1951; c) in *Excitation transfer*, in BARTON M. *et al.*, *Comparative Effects of Radiation* (Wiley, NY) 1960, pp. 300-319.

[5] DEXTER D. L., *J. Chem. Phys.*, **21** (1953) 836.

[6] a) BALZANI V., CREDI A. and VENTURI M., *ChemSusChem*, **1** (2008) 26; b) BLANKENSHIP R. E., *Molecular Mechanisms of Photosynthesis* (Blackwell Sci., Oxford) 2002.

[7] PULLERITS T. and SUNDSTRÖM V., *Acc. Chem. Res.*, **29** (1996) 381.

[8] a) CALZAFERRI G. and GFELLER N., *J. Phys. Chem.*, **96** (1992) 3428; b) BINDER F., CALZAFERRI G. and GFELLER N., *Sol. Energy Mater. Sol. Cells*, **38** (1995) 175; c) CALZAFERRI G., *Chimia*, **52** (1998) 525.

[9] GFELLER N. and CALZAFERRI G., *J. Phys. Chem. B*, **101** (1997) 1396.

[10] a) SCHULZ-EKLOFF G., WÖHRLE D., VAN DUFFEL B. and SCHOONHEYDT R. A., *Microporous Mesoporous Mater.*, **51** (2002) 91; b) HASHIMOTO S., *Photochem. Photobiol. C: Photochem. Rev.*, **4** (2003) 19; c) BEIN T., in *Studies in Surface Science and Catalysis*, Vol. **168**: *Introduction to Zeolite Science and Practice*, edited by CEJKA J., VAN BEKKUM H., CORMA A. and SCHÜTH F. (Elsevier, Amsterdam) 2007, 3d edition, pp. 611–658.

[11] a) MEGELSKI S. and CALZAFERRI G., *Adv. Funct. Mater.*, **11** (2001) 277; b) ZABALA RUIZ A., BRÜHWILER D., BAN T. and CALZAFERRI G., *Monatsh. Chem.*, **136** (2005) 77; c) ZABALA RUIZ A., BRÜHWILER D., DIEU L.-Q. and CALZAFERRI G., in *Materials Syntheses, A practical Guide*, edited by SCHUBERT U., HÜSING N. and LAINE R. (Springer, Wien) (ISBN 978-3-211-75124-4) 2008, pp. 1-9.

[12] a) BRECK D. W., *Zeolite Molecular Sieves* (John Wiley & Sons, NY) 1974; b) ERNST S. and WEITKAMP J., *Catal. Today*, **94** (1994) 27; c) BAERLOCHER CH., MEIER W. M. and OLSON D. H., *Atlas of Zeolite Framework Types* (Elsevier, Amsterdam) 2001, 5th edition; d) OHSUNA T., SLATER B., GAO F., YU J., SAKAMOTO Y., ZHU G., TERASAKI O., VAUGHAN D. E. W., QIU S. and CATLOW C. R. A., *Chem. Eur. J.*, **10** (2004) 5031; e) LARLUS O. and VALTCHEV V. P., *Chem. Mater.*, **16** (2004) 3381.

[13] a) Calzaferri G., Pauchard M., Maas H., Huber S., Khatyr A. and Schaafsma T., *J. Mater. Chem.*, **12** (2002) 1; b) Calzaferri G., Huber S., Maas H. and Minkowski C., *Angew. Chem. Int. Ed.*, **42** (2003) 3732; c) Brühwiler D. and Calzaferri G., *Microporous Mesoporous Mater.*, **72** (2004) 1.

[14] Davydov A. S., *Usp. Fiz. Nauk.*, **82** (1964) 145.

[15] a) McRae E. G. and Kasha M., in *Physical Progress in Radiation Biol.* (Academic Press, NY) 1964, pp. 23-42; b) Kasha M., *Radiat. Res.*, **20** (1963) 55; c) Kobayashi T., *J-Aggregates* (World Scientific, London) 1996; d) Lenhard J. R. and Hein B. R., *J. Phys. Chem.*, **100** (1996) 17287.

[16] a) Calzaferri G. and Lutkouskaya K., *Photochem. Photobiol. Sci.*, **7** (2008) 879; b) Calzaferri G., Li H. and Brühwiler D., *Chem. Eur. J.*, **14** (2008) 7442; c) Minkowski C. and Calzaferri G., *Angew. Chem. Int. Ed.*, **44** (2005) 5325.

[17] Busby M., Blum C., Tibben M., Fibikar S., Calzaferri G., Subramaniam V. and De Cola L., *J. Am. Chem. Soc.*, **130** (2008) 10970.

[18] a) Scholes G. D. and Fleming G. R., *J. Phys. Chem. B*, **104** (2000) 1854; b) Ortiz W., Krueger B. P., Kleiman V. D., Krause J. L. and Roitberg A. E., *J. Phys. Chem. B*, **109** (2005) 11512; c) Closs G. L., Piotrowiak P., MacInnis J. M. and Fleming G. R., *J. Am. Chem. Soc.*, **110** (1988) 2652.

[19] Sancho-García J. C., Brédas J.-L., Beljonne D., Cornil J., Martínes-Álvarez R., Hanack M., Poulsen L., Gierschner J., Mack H.-G., Egelhaaf H.-J. and Oelkrug D., *J. Phys. Chem. B*, **109** (2005) 4872.

[20] Fois E., Gamba A., Medici C. and Tabacchi G., *Chem.Phys.Chem.*, **6** (2005) 1917.

[21] Mulliken R. S., in *Selected papers of Mulliken R. S.*, edited by Ramsay D. A. and Hinze J. (Univ. Chicago Press, London) 1975, pp. 620-722.

[22] McGlynn S. P., Vanquickenborne L. G., Kinoshita M. and Carroll D. G., *Introduction to Applied Quantum Chemistry* (Holt, Rienehart and Winston, Inc., NY) 1972.

[23] Huber S. and Calzaferri G., *ChemPhysChem*, **5** (2004) 239.

[24] a) Zumofen G. and Blumen A., *J. Chem. Phys.*, **76** (1982) 3713; b) Anfinrud P., Crackel R. L. and Struve W. S., *J. Phys. Chem.*, **88** (1984) 5873; c) Tamai N., Yamazaki T. and Yamazaki I., *J. Phys. Chem.*, **91** (1987) 841; d) Kuhn H., *J. Chem. Phys.*, **53** (1970) 101; e) Valeur B., *Molecular Fluorescence* (Wiley-VCH, NY) 2002.

[25] Bossart O., De Cola L., Welter S. and Calzaferri G., *Chem. Eur. J.*, **10** (2004) 5771.

[26] Calzaferri G., Brühwiler D., Megelski S., Pfenniger M., Pauchard M., Hennessy B., Maas H., Devaux A. and Graf U., *Solid State Sci.*, **2** (2000) 421.

[27] a) Bücher H., Drexhage K. H., Fleck M., Kuhn H., Möbius D., Schäfer F. P., Sondermann J., Sperling W., Tillmann P. and Wiegand J., *Mol. Cryst.*, **2** (1967) 199; b) Kuhn H. and Möbius D., *Monolayer assemblies*, in *Physical Methods of Chemistry*, edited by Rossiter B. W. and Baetzold R. C., Vol. IXB (John Wiley & Sons, NY) 1993, 2nd edition, pp. 375-542; c) Grabowska J. and Sienicki K., *Chem. Phys.*, **192** (1995) 89; d) Webber S. E., *Chem. Rev.*, **90** (1990) 1469; e) Czikkely V., Försterling H. D. and Kuhn H., *Chem. Phys. Lett.*, **6** (1970) 11.

[28] Pauchard M., Huber S., Méallet-Renault R., Maas H., Pansu R. and Calzaferri G., *Angew. Chem. Int. Ed.*, **40** (2001) 2839.

[29] Yatskou M. M., Meyer M., Huber S., Pfenniger M. and Calzaferri G., *ChemPhysChem*, **4** (2003) 567.

[30] a) Farinha J. P. S., Spiro J. G. and Winnik M. A., *J. Phys. Chem. B*, **105** (2001) 4879; b) Hauser M., Klein U. K. A. and Gösele U., *Z. Phys. Chem.*, **101** (1976) 255.

[31] Lutkouskaya K. and Calzaferri G., *J. Phys. Chem. B*, **110** (2006) 5633.

[32] a) Maas H. and Calzaferri G., *Angew. Chem. Int. Ed.*, **41** (2002) 2284; b) Huber S. and Calzaferri G., *Angew. Chem. Int. Ed.*, **43** (2004) 6738.

[33] Zabala Ruiz A., Li H. and Calzaferri G., *Angew. Chem. Int. Ed.*, **45** (2006) 5282.